NANO LETTERS

pubs.acs.org/NanoLett

Nanopottery: Coiling of Electrospun Polymer Nanofibers

Ho-Young Kim,*,† Minhee Lee,† Kun Joong Park,† Sungho Kim,† and L. Mahadevan*,‡

†School of Mechanical and Aerospace Engineering, Seoul National University, Seoul 151-744, Korea, and ‡School of Engineering and Applied Sciences and Kavli Institute for Bionano Science and Technology, Harvard University, Cambridge, Massachusetts 02138

ABSTRACT We show that a nanoscale polymer solution electrojet can coil to form free-standing hollow pottery as the jet is focused onto a sharp electrode tip. A scaling law is given based on the balance of the electrostatic compression force and the elastic resistance to predict the coil radius and frequency as the functions of relevant physical parameters. The structures formed by the nanofibers can be used in diverse fields of nanotechnology, for example, as nanomagnets, bioscaffolds, and nanochannels.

KEYWORDS Coiling, electrospinning, nanofiber, jet stability, pottery, elasticity

The buckling, folding, and coiling of thin sheets and filaments of solids and fluids take place on length scales spanning several orders of magnitude, in phenomena ranging from orogenesis in geophysics to materials processing and soft-matter physics. For example, when an elastic rope is fed uniformly toward a horizontal plane, it first buckles and eventually coils into a spool that is deposited onto the plane.[1] A similar phenomenon also occurs when a slender viscous fluid jet impinges onto a horizontal plane and leads to the deposition of a liquid rope coil.[2] In either case, although the scale of the coil and the speed of coiling are determined by the balance between the internal elastic or viscous forces that resist deformation and a combination of inertia and gravity, the basic phenomenology is a consequence of geometry which favors bending deformations over stretching modes.

Here, we consider the spontaneous coiling of nanometric polymeric filaments that are electropsun onto a substrate to form regular cylindrical spools. When a polymer solution drop hanging from a capillary needle tip is subjected to a strong electrical field, a nanoscale jet is drawn out[3] and is attracted to the electrode. However, a bending instability of the electrified jet due to surface charges commonly leads to the chaotic deposition of nanofibers.[4] Attempts to stabilize the jet by reducing the distance between the plate ground and the liquid drop[5] or by placing a sharp ground tip adjacent to a collector plate[6] still resulted in the chaotic deposition of fibers on a stationary plate as shown in Figure 1. In the experiments, the nanofibers were electrospun onto (A) a conducting Al plate only 2 mm from the capillary tip and onto (B) a glass sheet at the same location as the Al plate with a sharp electrode tip underneath.

To prevent the jet instability, we finally used a sharp electrode tip near the liquid drop source with a strongly focused electrical field at the ground. This caused a stable jet to impinge on the tip and buckle and coil to yield a free-standing cylindrically spooled structure. Figure 2A shows the experimental setup, consisting of a syringe pump that supplies a polymer solution of poly(ethylene oxide) (PEO, molecular weight = 300000) to a metal capillary, a stainless steel conical ground with 50 μm in apex diameter situated 2 mm from the drop, a high voltage source, and a high-speed

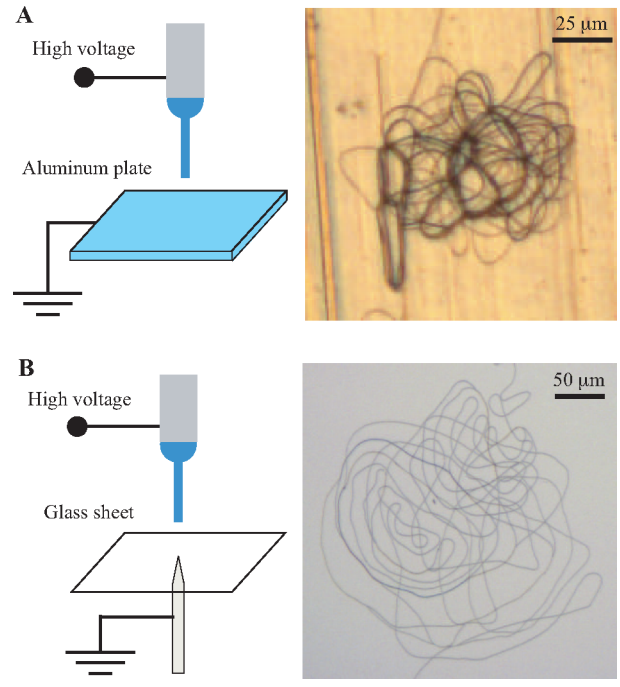

FIGURE 1. Chaotically deposited nanofibers as electrospun by the previously suggested focusing schemes. (A) Using an Al plate close to the capillary tip with the voltage difference of 1 kV. (B) Using a glass sheet with a sharp ground tip underneath. In both experiments, the jet duration was identically 0.7 s. Other experimental conditions are identical to those employed to yield the result of Figure 2.

*To whom correspondence should be addressed, hyk@snu.ac.kr and lm@seas.harvard.edu.

Received for review: 03/8/2010
Published on Web: 05/20/2010

DOI: 10.1021/nl100824d | *Nano Lett.* **2010,** *10,* 2138–2140

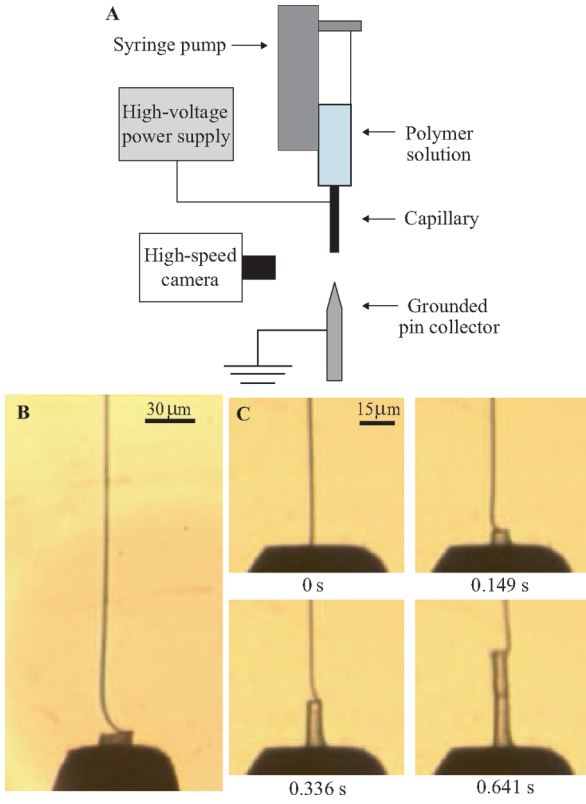

FIGURE 2. Experimental images of nanocoiling polymer fiber. (A) Schematic of the experimental apparatus. (B) A snapshot of a nanojet with 470 nm in final constant radius. (C) High-speed sequential images of a nanocoiling process that yields a free-standing hollow cylinder.

camera. In our experiments performed at room temperature and normal atmospheric pressure, an electrical jet is emitted from the drop when the electrical field strength exceeds approximately 1.2×10^6 V/m. The velocity and radius of the jet are functions of the viscosity of the drop, which depends on the initial PEO concentration (we used 6, 10, and 14 wt % of aqueous PEO solutions), the rate of evaporation, and the applied field, and yields a range of velocities, $U \in [1.5\ 30]$ mm/s and radii, $r \in [75\ 500]$ nm. As the solvent of the solutions, we used water purified by reverse osmosis. The permittivity of the initial aqueous solutions of PEO was measured, via open-ended sensors and reference liquid calibration,[7] to be 6.53×10^{-10}, 6.24×10^{-10}, and 5.97×10^{-10} F/m for PEO concentrations of 6%, 10%, and 14%, respectively.

Although the polymer solution is initially liquid, it starts to dry upon emerging as a drop of diameter $d \sim 1$ mm from the capillary and continues to dry as the jet flies through air. In our experiments, the solvent is estimated to have ample time to diffuse toward the fiber interface and evaporate into ambient air (Supporting Information). Hence, the jet is effectively a solid by the time it impinges on the target, as evidenced by the constant diameter of the jet shown in Figure 2B, and may be modeled as a thin elastic filament of radius ~50 nm even as it coils onto the tip ground. Figure 2C shows sequential images of the formation of a three-dimensional coiled structure of radius approximately 3 μm and height 40 μm as the jet whirls at a rate of ~10000 rpm, so that the entire structure is built in less than a second. In Figure 3 we show scanning electron microscopy images of hollow free-standing cylinders that might well have been shaped on a (nano) pottery wheel.

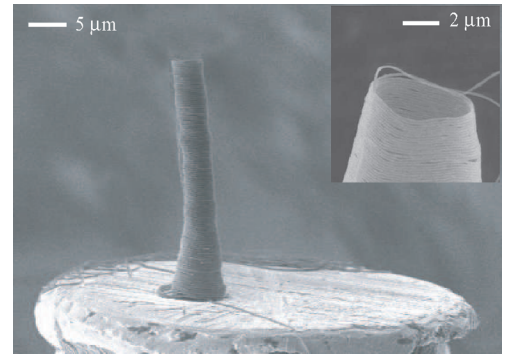

FIGURE 3. SEM images of the hollow coiled structure built on an apex of the stainless steel conical tip.

To characterize the coiling phenomenon and predict the radius of the coil R on relevant physical parameters, we consider the dominant forces acting on the fiber. The electrostatic force per unit fiber length F_e is scaled as $F_e \sim q_s r E$, where the electrical field strength $E \sim V/L$ with V being the electrical potential difference between the drop and the ground, separated by the distance L. The surface charge density q_s is scaled as $q_s \sim \varepsilon_0 E$, where $\varepsilon_0 = 8.854 \times 10^{-12}$ F/m is the permittivity of free space, provided that the fiber permittivity $\varepsilon \gg \varepsilon_0$.[8] The inertial forces scale as $F_i \sim \rho r^2 \Omega^2 R$, where ρ is the fiber density and Ω the angular frequency of coiling, and the gravitational forces per unit length scale as $F_g \sim \rho g r^2$, where g is the gravitational acceleration. Using typical experimental parameter values ($r \approx 100$ nm and $\rho \approx 1.21 \times 10^3$ kg/m^3), we find $F_i/F_e \sim 10^{-5}$ and $F_g/F_e \sim 10^{-4}$ so that F_i and F_g are negligibly small compared with F_e.

Then the spooling or coiling radius is determined by a balance between the electrostatic torque $F_e R^2$ and the elastic torque YI/R,[9] where Y is Young's modulus of a fiber and I the area moment of inertia ($\sim r^4$), so that

$$R \sim \left(\frac{Y}{\varepsilon_0 E^2}\right)^{1/3} r \tag{1}$$

The angular frequency of coiling Ω follows from mass conservation since $\Omega R = U$, so that

$$\Omega \sim \frac{U}{r}\left(\frac{\varepsilon_0 E^2}{Y}\right)^{1/3} \tag{2}$$

To test this prediction, we need to measure Young's modulus of a nanofiber as a function of solute (PEO) con-

DOI: 10.1021/nl100824d | Nano Lett. 2010, 10, 2138--2140

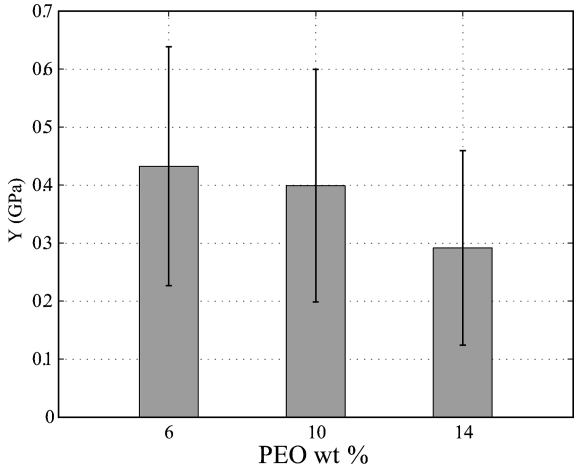

FIGURE 4. The averaged Young moduli of nanofibers with different PEO concentrations.

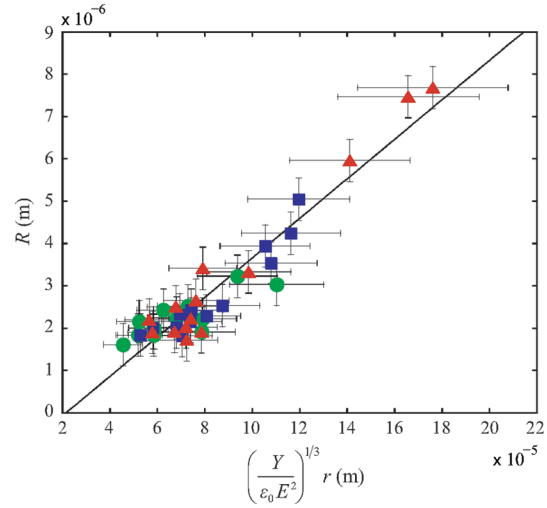

FIGURE 5. Coil radii plotted according to the scaling law (1). Circles, squares, and triangles correspond to 6, 10, and 14% of aqueous PEO solutions, respectively.

centration, a critical factor in determining the elasticity of these polymeric materials which move through a glass transition as a function of solute concentration. We deflected individual fibers hanging over a microtrench of width 30 μm and depth 3 μm (formed by deep etching of a silicon wafer) using an atomic force microscope (AFM) to measure Y, as delineated in Supporting Information. The measurement results allow us to find the dependency of the average modulus Y on PEO concentrations as shown in Figure 4.

The scaling law (1) states that the coil radius increases with fiber radius and/or with the electric field. In Figure 5 we plot the coil radius for a range of PEO concentrations in the solvent and the field E, as a function of the parameter $(Y/\varepsilon_0 E^2)^{1/3} r$, and see that the straight line fits $R \sim 0.05(Y/\varepsilon_0 E^2)^{1/3} r$, consistent with our simple scaling predictions.

In summary, we have shown that coiling of nanoscale fibers can arise as an electrospun polymer solution jet is focused onto a sharp electrode tip, leading to a stable hollow helical structure. A simple scaling law captures the physics of the process and enables us to start thinking about the control of the coil geometry using experimental parameters. The regular geometry of coiling microstructures may be of use in nanoscale magnets, in building nanotextured surfaces for bioscaffolds and nanochannels, and in other functional structures. An array of electrode target spots on an insulating substrate that are turned on sequentially may provide a viable solution to fabricate two-dimensional arrays of coiling microstructures because it can prevent electric field interference. Further study for fabrication of multiple spools on an array of target spots using different solutions will be crucial in realizing the wide application of this nanocoiling process.

Acknowledgment. This work was supported by KOSEF (R01-2006-000-10444-0) and KRF (412-J03001), and administered by SNU-IAMD.

Note Added after ASAP Publication. This paper published ASAP May 20, 2010 without the Acknowledgment section; the corrected version published ASAP May 25, 2010; L. Mahadevan's affiliation was updated on June 9, 2010.

Supporting Information Available. Estimation of solvent evaporation and measurement of Young's modulus. This material is available free of charge via the Internet at http://pubs.acs.org.

REFERENCES AND NOTES

(1) Mahadevan, L.; Keller, J. B. *Proc. R. Soc. London, Ser. A* **1996**, *452*, 1679.
(2) Mahadevan, L.; Ryu, W. S.; Samuel, D. T. *Nature* **1998**, *392*, 140. Mahadevan, L.; Ryu, W. S.; Samuel, D. T. *Nature* **2000**, *403*, 502.
(3) Reneker, D. H.; Yarin, A. L. *Polymer* **2008**, *49*, 2387.
(4) Reneker, D. H.; Yarin, A. L.; Fong, H.; Koombhongse, S. *J. Appl. Phys.* **2000**, *87*, 4531.
(5) Sun, D.; Chang, C.; Li, S.; Lin, L. *Nano Lett.* **2006**, *6*, 839.
(6) Yu, J.; Qiu, Y.; Zha, X.; Yu, M.; Yu, J.; Rafique, J.; Yin, J. *Eur. Polym. J.* **2008**, *44*, 2838.
(7) Nyshadham, A.; Sibbald, C. L.; Stuchly, S. S. *IEEE Trans. Microwave Theory Tech.* **1992**, *40*, 305.
(8) Haus, H. A.; Melcher, J. R. *Electromagnetic Fields and Energy*; Pentice-Hall: Englewood Cliffs, NJ, 1989.
(9) Landau, L. D.; Lifshitz, E. M. *Theory of Elasticity*, 3rd ed.; Butterworth-Heinemann: London, 1986.

DOI: 10.1021/nl100824d | *Nano Lett.* **2010,** *10,* 2138--2140

Supporting Information for
"Nanopottery: Coiling of electrospun polymer nanofibers"

1. Estimation of solvent evaporation

The evaporation of the polymer solution begins when it emerges from the capillary as a drop of the diameter $d \approx 1$ mm and continues in the flight as a nanojet. For the solvent (water) to evaporate into the surrounding air, the solvent molecules must travel through the solution and then leave the air/fiber interface. Therefore, the evaporation process consists of internal diffusion and external convection. The mass transfer Biot number, Bi, measures the relative magnitude of the internal diffusion resistance to the external convection resistance:

$$Bi = \frac{hl\alpha}{D} \tag{1}$$

where h is the convective mass transfer coefficient, l the length scale over which the solvent must move through in the solution to reach the air/fiber interface, α the partition coefficient between the two phases at the interface, D the internal solvent diffusion coefficient. The value of α is estimated as the ratio of the partial densities of the solvent on the liquid and the vapor side, $\alpha \sim 10^{-3}$. D is known to greatly depend on the solvent concentration, but we take a representative order of magnitude of $D \sim 10^{-11}$ m^2/s following [1]. The value of h depends on the geometry and the velocity of the polymer solution. Thus we first consider the evaporation when the solution is in a drop and then proceed to the case when the solution is in a nanojet.

We start with the rate of evaporation in the drop waiting to form the Taylor cone jet before the electrical field is applied. For a stationary drop, the Sherwood number (the ratio of convective to diffusive mass transport), $Sh = hd/D_v \approx 2$,[2] gives the value of $h \approx 2D_v/d$, where D_v is the water vapor diffusion coefficient through the air and normally taken to be $D_v \sim 10^{-5}$ m^2/s. Then for a drop of $d \approx 1$ mm, $h \approx 0.02$ m/s. The mass transfer Biot number for the drop, $Bi \sim 10^3 \gg 1$ with $l = d$. For a jet, $Sh = 2hr/D_v \approx 0.3$[1] with r being the jet radius ($r \approx 500$ nm for the jet in Fig. 2). Therefore, we get $h \sim 3$ m/s, which leads to $Bi \sim 300 \gg 1$ with $l = 2r$. The fact that $Bi \gg 1$ implies that the internal diffusive resistance dominates over the convective process. Therefore, the internal diffusion controls the solvent removal process and the resistance due to convection can be neglected.

Now we estimate the thickness of the boundary layer of the solvent concentration formed

at the skin of the solution either in a drop or a fiber (jet). The thickness of diffusive boundary layers can be scaled as $\delta \sim (Dt)^{1/2}$, where t is time. In our experiments, the longer the drop is exposed to air before a jet is ensued, the more stable becomes the jet. This is presumably due to solvent evaporation that increases the solution viscosity that impedes the abrupt jet bending, if any. In each run, we waited 30 s since the drop was formed at the metal capillary before the electrical field was applied. In this period, the concentration boundary layer thickness grows as large as $\delta \sim 10$ μm. Considering that the solution at the drop/air interface (or the skin of the drop) is drawn out to become the Taylor cone jet, the jet whose diameter is about 1 μm is already significantly dried. While the polymer fiber (or jet) travels toward the target ground, the solvent continues to evaporate. The duration of the travel is simply given by $t = L/U$, where $L = 2$ mm and $U = 3$ mm/s, so that $t = 0.7$ s. Then the simply estimated boundary layer thickness is $\delta \sim (0.7 \times 10^{-11})^{1/2} \sim 3$ μm, which is larger than the actual fiber radius, 500 nm. In other words, the characteristic boundary layer thickness δ becomes equal to the fiber radius r, when the fiber travels by $L_f = Ur^2/D \sim 100$ μm $< L$, i.e. well before the fiber reaches the target.

Our scaling analysis for the solvent evaporation in the electrospinning process employed in the experiments reveals that the solvent has ample time to diffuse toward the fiber interface and evaporate into ambient air. Thus the jet is effectively a solid by the time it impinges on the target. This is experimentally verified by the fact that the jet diameter does not change during flight as shown in Fig. 2B. If the jet behaved as a liquid jet, the cross-section should have decreased downstream due to jet elongation (caused by the downward acceleration) and continuous solvent evaporation.

2. Measurement of Young's modulus

We deflected individual fibers hanging over a microtrench of the width 30 μm and depth 3 μm (formed by deep etching of a silicon wafer) using an atomic force microscope (AFM), as shown in Figure 1, a similar method adopted by Bellan et al.[3] The fiber deflection v is given by $v = (w - w_0) - \Delta w$, and it is related to the force of the cantilever tip, P, as $P = 8AY(v/b)$, where A and b are the cross-sectional area and the length of the nanofiber, respectively. The measurement results allow us to find the dependency of the average modulus Y on PEO concentrations as shown in Figure 1C.

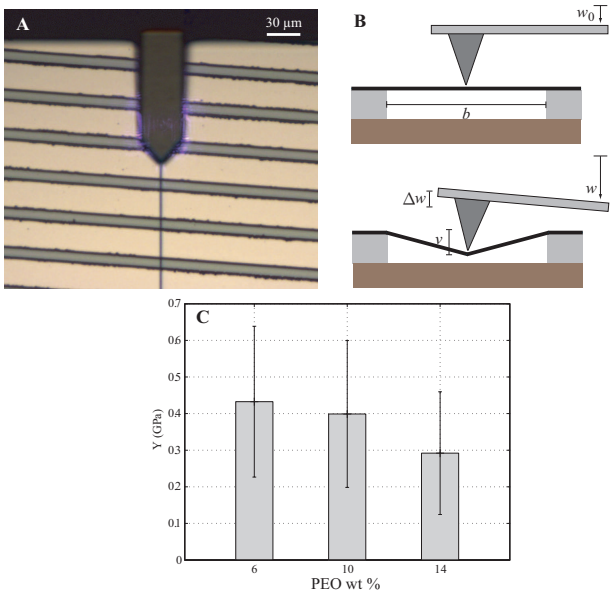

Figure 1: Measuring Young's modulus with AFM. A: Top view of an AFM probe and a nanofiber hanging over microtrenches. B: Measurement schematic of nanofiber deflection using an AFM probe. C: The averaged Young moduli of nanofibers with different PEO concentrations.

References

[1] Kojic, N.; Kojic, M.; Gudlavalleti, S.; McKinley, G. *Biomacromolecules* **2004**, *5*, 1698.

[2] Incropera, F. P.; DeWitt, D. P. *Fundamentals of Heat and Mass Transfer*, 5th ed. **2002**.

[3] Bellan, L. M.; Kameoka, J.; Craighead, H. G. *Nanotechnology* **2005**, *16*, 1095.

RESEARCH HIGHLIGHTS

GEOPHYSICS

Glaciers going, going...

Geophys. Res. Lett. doi:10.1029/2010GL042616 (2010)
As much as half of the glacial retreat documented in the Swiss Alps in recent decades could be due to natural cycles in the North Atlantic climate.

Matthias Huss at the Swiss Federal Institute of Technology in Zurich and his co-authors combined field data with computer modelling to develop a 100-year record of glacier surface mass balance from 1908 to 2008. The team compared their records with global climate data as well as with regional climate trends relating to multidecadal oscillations in Atlantic Ocean surface temperatures.

The findings may help to sharpen predictions of the impact of future climate change on glaciers, the authors say. **J.T.**

S. MCDERMOTT/CORBIS

ASTRONOMY

Clouds with an H_2 lining

Astrophys. J. **715,** 1370–1382 (2010)
Stars are born inside giant clouds of gas. Figuring out where such clouds begin and end is tricky because their main component, molecular hydrogen (H_2), is often too cold to be seen by telescopes.

Paul Goldsmith and his colleagues at NASA's Jet Propulsion Laboratory in Pasadena, California, have used the orbiting Spitzer Space Telescope to find the edge of a nearby molecular cloud. By detecting emissions from transitions in the rotational states of molecular hydrogen, they found hints of a warm layer of H_2 on the surface of the cloud. The team suggests that the properties of the hot edge could be related to circulation of gas within the cloud. **G.B.**

ECOLOGY

What's that whale?

Genome Res. doi:10.1101/gr.102954.109 (2010)
Killer whales consist of several species, not just one, according to a genetic study.

Different populations or 'ecotypes' of killer whale (*Orcinus orca*) vary in traits such as body size, social structure and preferred prey. Yet analyses of fragments of their mitochondrial DNA — which is inherited only from the mother and is often studied to delineate species — have revealed very low levels of genetic diversity between ecotypes, probably because of low mutation rates.

Phillip Morin of the National Marine Fisheries Service in La Jolla, California, and his colleagues examined the entire mitochondrial genome of 139 whales from the North Pacific, North Atlantic and Southern oceans. The authors found enough genetic variation to suggest renaming three of the ecotypes as separate species and classifying the rest as subspecies until more data become available. **L.O.-S.**

NANOMANUFACTURING

Petite pottery

Nano Lett. doi:10.1021/nl100824d (2010)
Polymer nanofibres can be spun into free-standing, hollow cylinders that look as if they might have been shaped on a tiny pottery wheel. Ho-Young Kim at Seoul National University, L. Mahadevan at Harvard University in Cambridge, Massachusetts, and their co-workers used an electric field to tease a nanometre-scale jet of polyethylene oxide solution from a capillary tube. The jet dried in mid-air and, in less than a second, coiled up into a spool a few micrometres in diameter (pictured) as it hit a sharp stainless steel tip 2 millimetres below the capillary tube.

Such structures could be used in nanometre-scale magnets, bioscaffolds or nanochannels, the researchers suggest. **R.V.N.**

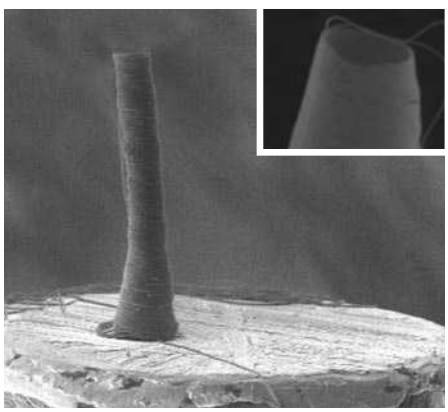

PHYSIOLOGY

Marathon metabolites

Science Trans. Med. **2,** 33ra37 (2010)
An analysis of 210 blood metabolites has yielded indicators of physical fitness.

Robert Gerszten and Gregory Lewis at Massachusetts General Hospital in Boston and their colleagues analysed blood samples taken from 70 people before and after a ten-minute run on a treadmill. The researchers found that, across the group, the levels of 21 metabolites changed during the run. Some of these metabolites are linked to cardiovascular fitness and faster running times in the Boston Marathon. Furthermore, fit volunteers showed signs of having more efficient fat metabolism than less fit individuals.

Feeding cultured cells a mixture of five of the 21 metabolites — glycerol, niacinamide, glucose-6-phosphate, pantothenate and succinate — rapidly boosted expression of the NUR77 protein, which controls glucose and lipid metabolism in muscles. **H.L.**

For a longer story on this research, see go.nature.com/g5P4Pb

GENOMICS

Transposition trends

Genome Res. doi:10.1101/gr.106419.110 (2010)
Researchers have mapped the genomic locations of almost every member of a family of human retrotransposons — short DNA segments thought to make up as much as one-third of the genome. These elements — which can affect physical traits — copy and then paste themselves back into the genome at various locations. Despite their abundance, they are not as well studied as other forms of genomic variation.

AM. CHEM. SOC.